



Searches for Λ_b^0 and Ξ_b^0 decays to $K_s^0 p \pi^-$ and $K_s^0 p K^-$ final states with first observation of the $\Lambda_b^0 \rightarrow K_s^0 p \pi^-$ decay

The LHCb collaboration[†]

Abstract

A search for previously unobserved decays of beauty baryons to the final states $K_s^0 p \pi^-$ and $K_s^0 p K^-$ is reported. The analysis is based on a data sample corresponding to an integrated luminosity of 1.0 fb^{-1} of pp collisions. The $\Lambda_b^0 \rightarrow \bar{K}^0 p \pi^-$ decay is observed with a significance of 8.6σ , with branching fraction

$$\mathcal{B}(\Lambda_b^0 \rightarrow \bar{K}^0 p \pi^-) = (1.26 \pm 0.19 \pm 0.09 \pm 0.34 \pm 0.05) \times 10^{-5},$$

where the uncertainties are statistical, systematic, from the ratio of fragmentation fractions $f_{\Lambda_b^0}/f_d$, and from the branching fraction of the $B^0 \rightarrow K^0 \pi^+ \pi^-$ normalisation channel, respectively. A first measurement is made of the CP asymmetry, giving

$$A_{CP}(\Lambda_b^0 \rightarrow \bar{K}^0 p \pi^-) = 0.22 \pm 0.13 (\text{stat}) \pm 0.03 (\text{syst}).$$

No significant signals are seen for $\Lambda_b^0 \rightarrow K_s^0 p K^-$ decays, Ξ_b^0 decays to both the $K_s^0 p \pi^-$ and $K_s^0 p K^-$ final states, and the $\Lambda_b^0 \rightarrow D_s^- (\rightarrow K_s^0 K^-) p$ decay, and upper limits on their branching fractions are reported.

Submitted to JHEP

© CERN on behalf of the LHCb collaboration, license CC-BY-3.0.

[†]Authors are listed on the following pages.

LHCb collaboration

R. Aaij⁴⁰, B. Adeva³⁶, M. Adinolfi⁴⁵, A. Affolder⁵¹, Z. Ajaltouni⁵, J. Albrecht⁹, F. Alessio³⁷, M. Alexander⁵⁰, S. Ali⁴⁰, G. Alkhazov²⁹, P. Alvarez Cartelle³⁶, A.A. Alves Jr²⁴, S. Amato², S. Amerio²¹, Y. Amhis⁷, L. Anderlini^{17,g}, J. Anderson³⁹, R. Andreassen⁵⁶, M. Andreotti^{16,f}, J.E. Andrews⁵⁷, R.B. Appleby⁵³, O. Aquines Gutierrez¹⁰, F. Archilli³⁷, A. Artamonov³⁴, M. Artuso⁵⁸, E. Aslanides⁶, G. Auriemma^{24,n}, M. Baalouch⁵, S. Bachmann¹¹, J.J. Back⁴⁷, A. Badalov³⁵, V. Balagura³⁰, W. Baldini¹⁶, R.J. Barlow⁵³, C. Barschel³⁸, S. Barsuk⁷, W. Barter⁴⁶, V. Batozskaya²⁷, Th. Bauer⁴⁰, A. Bay³⁸, J. Beddow⁵⁰, F. Bedeschi²², I. Bediaga¹, S. Belogurov³⁰, K. Belous³⁴, I. Belyaev³⁰, E. Ben-Haim⁸, G. Bencivenni¹⁸, S. Benson⁴⁹, J. Benton⁴⁵, A. Berezhnoy³¹, R. Bernet³⁹, M.-O. Bettler⁴⁶, M. van Beuzekom⁴⁰, A. Bien¹¹, S. Bifani⁴⁴, T. Bird⁵³, A. Bizzeti^{17,i}, P.M. Bjørnstad⁵³, T. Blake⁴⁷, F. Blanc³⁸, J. Blouw¹⁰, S. Blusk⁵⁸, V. Bocci²⁴, A. Bondar³³, N. Bondar²⁹, W. Bonivento^{15,37}, S. Borghi⁵³, A. Borgia⁵⁸, M. Borsato⁷, T.J.V. Bowcock⁵¹, E. Bowen³⁹, C. Bozzi¹⁶, T. Brambach⁹, J. van den Brand⁴¹, J. Bressieux³⁸, D. Brett⁵³, M. Britsch¹⁰, T. Britton⁵⁸, N.H. Brook⁴⁵, H. Brown⁵¹, A. Bursche³⁹, G. Busetto^{21,r}, J. Buytaert³⁷, S. Cadeddu¹⁵, R. Calabrese^{16,f}, O. Callot⁷, M. Calvi^{20,k}, M. Calvo Gomez^{35,p}, A. Camboni³⁵, P. Campana^{18,37}, D. Campora Perez³⁷, A. Carbone^{14,d}, G. Carboni^{23,l}, R. Cardinale^{19,j}, A. Cardini¹⁵, H. Carranza-Mejia⁴⁹, L. Carson⁴⁹, K. Carvalho Akiba², G. Casse⁵¹, L. Castillo Garcia³⁷, M. Cattaneo³⁷, Ch. Cauet⁹, R. Cenci⁵⁷, M. Charles⁸, Ph. Charpentier³⁷, S.-F. Cheung⁵⁴, N. Chiapolini³⁹, M. Chrzaszcz^{39,25}, K. Ciba³⁷, X. Cid Vidal³⁷, G. Ciezarek⁵², P.E.L. Clarke⁴⁹, M. Clemencic³⁷, H.V. Cliff⁴⁶, J. Closier³⁷, C. Coca²⁸, V. Coco³⁷, J. Cogan⁶, E. Cogneras⁵, P. Collins³⁷, A. Comerma-Montells³⁵, A. Contu^{15,37}, A. Cook⁴⁵, M. Coombes⁴⁵, S. Coquereau⁸, G. Corti³⁷, B. Couturier³⁷, G.A. Cowan⁴⁹, D.C. Craik⁴⁷, M. Cruz Torres⁵⁹, S. Cunliffe⁵², R. Currie⁴⁹, C. D'Ambrosio³⁷, J. Dalseno⁴⁵, P. David⁸, P.N.Y. David⁴⁰, A. Davis⁵⁶, I. De Bonis⁴, K. De Bruyn⁴⁰, S. De Capua⁵³, M. De Cian¹¹, J.M. De Miranda¹, L. De Paula², W. De Silva⁵⁶, P. De Simone¹⁸, D. Decamp⁴, M. Deckenhoff⁹, L. Del Buono⁸, N. Déléage⁴, D. Derkach⁵⁴, O. Deschamps⁵, F. Dettori⁴¹, A. Di Canto¹¹, H. Dijkstra³⁷, S. Donleavy⁵¹, F. Dordei¹¹, P. Dorosz^{25,o}, A. Dosil Suárez³⁶, D. Dossett⁴⁷, A. Dovbnya⁴², F. Dupertuis³⁸, P. Durante³⁷, R. Dzhelyadin³⁴, A. Dziurda²⁵, A. Dzyuba²⁹, S. Easo⁴⁸, U. Egede⁵², V. Egorychev³⁰, S. Eidelman³³, D. van Eijk⁴⁰, S. Eisenhardt⁴⁹, U. Eitschberger⁹, R. Ekelhof⁹, L. Eklund^{50,37}, I. El Rifai⁵, Ch. Elsasser³⁹, A. Falabella^{16,f}, C. Färber¹¹, C. Farinelli⁴⁰, S. Farry⁵¹, D. Ferguson⁴⁹, V. Fernandez Albor³⁶, F. Ferreira Rodrigues¹, M. Ferro-Luzzi³⁷, S. Filippov³², M. Fiore^{16,f}, M. Fiorini^{16,f}, C. Fitzpatrick³⁷, M. Fontana¹⁰, F. Fontanelli^{19,j}, R. Forty³⁷, O. Francisco², M. Frank³⁷, C. Frei³⁷, M. Frosini^{17,37,g}, E. Furfaro^{23,l}, A. Gallas Torreira³⁶, D. Galli^{14,d}, M. Gandelman², P. Gandini⁵⁸, Y. Gao³, J. Garofoli⁵⁸, P. Garosi⁵³, J. Garra Tico⁴⁶, L. Garrido³⁵, C. Gaspar³⁷, R. Gauld⁵⁴, E. Gersabeck¹¹, M. Gersabeck⁵³, T. Gershon⁴⁷, Ph. Ghez⁴, A. Gianelle²¹, V. Gibson⁴⁶, L. Giubega²⁸, V.V. Gligorov³⁷, C. Göbel⁵⁹, D. Golubkov³⁰, A. Golutvin^{52,30,37}, A. Gomes^{1,a}, H. Gordon³⁷, M. Grabalosa Gándara⁵, R. Graciani Diaz³⁵, L.A. Granado Cardoso³⁷, E. Graugés³⁵, G. Graziani¹⁷, A. Greco²⁸, E. Greening⁵⁴, S. Gregson⁴⁶, P. Griffith⁴⁴, L. Grillo¹¹, O. Grünberg⁶⁰, B. Gui⁵⁸, E. Gushchin³², Yu. Guz^{34,37}, T. Gys³⁷, C. Hadjivasiliou⁵⁸, G. Haefeli³⁸, C. Haen³⁷, T.W. Hafkenscheid⁶², S.C. Haines⁴⁶, S. Hall⁵², B. Hamilton⁵⁷, T. Hampson⁴⁵, S. Hansmann-Menzemer¹¹, N. Harnew⁵⁴, S.T. Harnew⁴⁵, J. Harrison⁵³, T. Hartmann⁶⁰, J. He³⁷, T. Head³⁷, V. Heijne⁴⁰, K. Hennessy⁵¹, P. Henrard⁵, J.A. Hernando Morata³⁶, E. van Herwijnen³⁷, M. Heß⁶⁰, A. Hicheur¹, D. Hill⁵⁴, M. Hoballah⁵, C. Hombach⁵³, W. Hulsbergen⁴⁰, P. Hunt⁵⁴, T. Huse⁵¹, N. Hussain⁵⁴, D. Hutchcroft⁵¹,

D. Hynds⁵⁰, V. Iakovenko⁴³, M. Idzik²⁶, P. Ilten⁵⁵, R. Jacobsson³⁷, A. Jaeger¹¹, E. Jans⁴⁰,
 P. Jatón³⁸, A. Jawahery⁵⁷, F. Jing³, M. John⁵⁴, D. Johnson⁵⁴, C.R. Jones⁴⁶, C. Joram³⁷,
 B. Jost³⁷, N. Jurik⁵⁸, M. Kaballo⁹, S. Kandybei⁴², W. Kanso⁶, M. Karacson³⁷, T.M. Karbach³⁷,
 I.R. Kenyon⁴⁴, T. Ketel⁴¹, B. Khanji²⁰, S. Klaver⁵³, O. Kochebina⁷, I. Komarov³⁸,
 R.F. Koopman⁴¹, P. Koppenburg⁴⁰, M. Korolev³¹, A. Kozlinskiy⁴⁰, L. Kravchuk³², K. Kreplin¹¹,
 M. Kreps⁴⁷, G. Krocker¹¹, P. Krokovny³³, F. Kruse⁹, M. Kucharczyk^{20,25,37,k}, V. Kudryavtsev³³,
 K. Kurek²⁷, T. Kvaratskheliya^{30,37}, V.N. La Thi³⁸, D. Lacarrere³⁷, G. Lafferty⁵³, A. Lai¹⁵,
 D. Lambert⁴⁹, R.W. Lambert⁴¹, E. Lanciotti³⁷, G. Lanfranchi¹⁸, C. Langenbruch³⁷,
 T. Latham⁴⁷, C. Lazzeroni⁴⁴, R. Le Gac⁶, J. van Leerdam⁴⁰, J.-P. Lees⁴, R. Lefèvre⁵,
 A. Leflat³¹, J. Lefrançois⁷, S. Leo²², O. Leroy⁶, T. Lesiak²⁵, B. Leverington¹¹, Y. Li³, M. Liles⁵¹,
 R. Lindner³⁷, C. Linn¹¹, F. Lionetto³⁹, B. Liu¹⁵, G. Liu³⁷, S. Lohn³⁷, I. Longstaff⁵⁰, J.H. Lopes²,
 N. Lopez-March³⁸, P. Lowdon³⁹, H. Lu³, D. Lucchesi^{21,r}, J. Luisier³⁸, H. Luo⁴⁹, E. Luppi^{16,f},
 O. Lupton⁵⁴, F. Machefert⁷, I.V. Machikhiliyan³⁰, F. Maciuc²⁸, O. Maev^{29,37}, S. Malde⁵⁴,
 G. Manca^{15,e}, G. Mancinelli⁶, J. Maratas⁵, U. Marconi¹⁴, P. Marino^{22,t}, R. Märki³⁸, J. Marks¹¹,
 G. Martellotti²⁴, A. Martens⁸, A. Martín Sánchez⁷, M. Martinelli⁴⁰, D. Martinez Santos⁴¹,
 D. Martins Tostes², A. Massafferri¹, R. Matev³⁷, Z. Mathe³⁷, C. Matteuzzi²⁰, A. Mazurov^{16,37,f},
 M. McCann⁵², J. McCarthy⁴⁴, A. McNab⁵³, R. McNulty¹², B. McSkelly⁵¹, B. Meadows^{56,54},
 F. Meier⁹, M. Meissner¹¹, M. Merk⁴⁰, D.A. Milanes⁸, M.-N. Minard⁴, J. Molina Rodriguez⁵⁹,
 S. Monteil⁵, D. Moran⁵³, M. Morandin²¹, P. Morawski²⁵, A. Mordà⁶, M.J. Morello^{22,t},
 R. Mountain⁵⁸, I. Mous⁴⁰, F. Muheim⁴⁹, K. Müller³⁹, R. Muresan²⁸, B. Muryn²⁶, B. Muster³⁸,
 P. Naik⁴⁵, T. Nakada³⁸, R. Nandakumar⁴⁸, I. Nasteva¹, M. Needham⁴⁹, S. Neubert³⁷,
 N. Neufeld³⁷, A.D. Nguyen³⁸, T.D. Nguyen³⁸, C. Nguyen-Mau^{38,q}, M. Nicol⁷, V. Niess⁵,
 R. Niet⁹, N. Nikitin³¹, T. Nikodem¹¹, A. Novoselov³⁴, A. Oblakowska-Mucha²⁶, V. Obraztsov³⁴,
 S. Oggero⁴⁰, S. Ogilvy⁵⁰, O. Okhrimenko⁴³, R. Oldeman^{15,e}, G. Onderwater⁶², M. Orlandea²⁸,
 J.M. Otalora Goicochea², P. Owen⁵², A. Oyanguren³⁵, B.K. Pal⁵⁸, A. Palano^{13,c}, M. Palutan¹⁸,
 J. Panman³⁷, A. Papanestis^{48,37}, M. Pappagallo⁵⁰, L. Pappalardo¹⁶, C. Parkes⁵³,
 C.J. Parkinson⁹, G. Passaleva¹⁷, G.D. Patel⁵¹, M. Patel⁵², C. Patrignani^{19,j},
 C. Pavel-Nicorescu²⁸, A. Pazos Alvarez³⁶, A. Pearce⁵³, A. Pellegrino⁴⁰, G. Penso^{24,m},
 M. Pepe Altarelli³⁷, S. Perazzini^{14,d}, E. Perez Trigo³⁶, P. Perret⁵, M. Perrin-Terrin⁶,
 L. Pescatore⁴⁴, E. Pesen⁶³, G. Pessina²⁰, K. Petridis⁵², A. Petrolini^{19,j}, E. Picatoste Olloqui³⁵,
 B. Pietrzyk⁴, T. Pilar⁴⁷, D. Pinci²⁴, A. Pistone¹⁹, S. Playfer⁴⁹, M. Plo Casasus³⁶, F. Polci⁸,
 G. Polok²⁵, A. Poluektov^{47,33}, E. Polycarpo², A. Popov³⁴, D. Popov¹⁰, B. Popovici²⁸,
 C. Potterat³⁵, A. Powell⁵⁴, J. Prisciandaro³⁸, A. Pritchard⁵¹, C. Prouve⁴⁵, V. Pugatch⁴³,
 A. Puig Navarro³⁸, G. Punzi^{22,s}, W. Qian⁴, B. Rachwal²⁵, J.H. Rademacker⁴⁵,
 B. Rakotomiamanana³⁸, M. Rama¹⁸, M.S. Rangel², I. Raniuk⁴², N. Rauschmayr³⁷,
 G. Raven⁴¹, S. Redford⁵⁴, S. Reichert⁵³, M.M. Reid⁴⁷, A.C. dos Reis¹, S. Ricciardi⁴⁸,
 A. Richards⁵², K. Rinnert⁵¹, V. Rives Molina³⁵, D.A. Roa Romero⁵, P. Robbe⁷, D.A. Roberts⁵⁷,
 A.B. Rodrigues¹, E. Rodrigues⁵³, P. Rodriguez Perez³⁶, S. Roiser³⁷, V. Romanovsky³⁴,
 A. Romero Vidal³⁶, M. Rotondo²¹, J. Rouvinet³⁸, T. Ruf³⁷, F. Ruffini²², H. Ruiz³⁵,
 P. Ruiz Valls³⁵, G. Sabatino^{24,l}, J.J. Saborido Silva³⁶, N. Sagidova²⁹, P. Sail⁵⁰, B. Saitta^{15,e},
 V. Salustino Guimaraes², B. Sanmartin Sedes³⁶, R. Santacesaria²⁴, C. Santamarina Rios³⁶,
 E. Santovetti^{23,l}, M. Sapunov⁶, A. Sarti¹⁸, C. Satriano^{24,n}, A. Satta²³, M. Savrie^{16,f},
 D. Savrina^{30,31}, M. Schiller⁴¹, H. Schindler³⁷, M. Schlupp⁹, M. Schmelling¹⁰, B. Schmidt³⁷,
 O. Schneider³⁸, A. Schopper³⁷, M.-H. Schune⁷, R. Schwemmer³⁷, B. Sciascia¹⁸, A. Sciubba²⁴,
 M. Seco³⁶, A. Semennikov³⁰, K. Senderowska²⁶, I. Sepp⁵², N. Serra³⁹, J. Serrano⁶, P. Seyfert¹¹,
 M. Shapkin³⁴, I. Shapoval^{16,42,f}, Y. Shcheglov²⁹, T. Shears⁵¹, L. Shekhtman³³, O. Shevchenko⁴²,

V. Shevchenko⁶¹, A. Shires⁹, R. Silva Coutinho⁴⁷, G. Simi²¹, M. Sirendi⁴⁶, N. Skidmore⁴⁵, T. Skwarnicki⁵⁸, N.A. Smith⁵¹, E. Smith^{54,48}, E. Smith⁵², J. Smith⁴⁶, M. Smith⁵³, H. Snoek⁴⁰, M.D. Sokoloff⁵⁶, F.J.P. Soler⁵⁰, F. Soomro³⁸, D. Souza⁴⁵, B. Souza De Paula², B. Spaan⁹, A. Sparkes⁴⁹, P. Spradlin⁵⁰, F. Stagni³⁷, S. Stahl¹¹, O. Steinkamp³⁹, S. Stevenson⁵⁴, S. Stoica²⁸, S. Stone⁵⁸, B. Storaci³⁹, S. Stracka^{22,37}, M. Straticiuc²⁸, U. Straumann³⁹, R. Stroili²¹, V.K. Subbiah³⁷, L. Sun⁵⁶, W. Sutcliffe⁵², S. Swientek⁹, V. Syropoulos⁴¹, M. Szczekowski²⁷, P. Szczypka^{38,37}, D. Szilard², T. Szumlak²⁶, S. T'Jampens⁴, M. Teklishyn⁷, G. Tellarini^{16,f}, E. Teodorescu²⁸, F. Teubert³⁷, C. Thomas⁵⁴, E. Thomas³⁷, J. van Tilburg¹¹, V. Tisserand⁴, M. Tobin³⁸, S. Tolk⁴¹, L. Tomassetti^{16,f}, D. Tonelli³⁷, S. Topp-Joergensen⁵⁴, N. Tori⁵⁴, E. Tournefier^{4,52}, S. Tourneur³⁸, M.T. Tran³⁸, M. Tresch³⁹, A. Tsaregorodtsev⁶, P. Tsopelas⁴⁰, N. Tuning⁴⁰, M. Ubeda Garcia³⁷, A. Ukleja²⁷, A. Ustyuzhanin⁶¹, U. Uwer¹¹, V. Vagnoni¹⁴, G. Valenti¹⁴, A. Vallier⁷, R. Vazquez Gomez¹⁸, P. Vazquez Regueiro³⁶, C. Vázquez Sierra³⁶, S. Vecchi¹⁶, J.J. Velthuis⁴⁵, M. Veltri^{17,h}, G. Veneziano³⁸, M. Vesterinen¹¹, B. Viaud⁷, D. Vieira², X. Vilasis-Cardona^{35,p}, A. Vollhardt³⁹, D. Volyanskyy¹⁰, D. Voong⁴⁵, A. Vorobyev²⁹, V. Vorobyev³³, C. Vob⁶⁰, H. Voss¹⁰, J.A. de Vries⁴⁰, R. Waldi⁶⁰, C. Wallace⁴⁷, R. Wallace¹², S. Wandernoth¹¹, J. Wang⁵⁸, D.R. Ward⁴⁶, N.K. Watson⁴⁴, A.D. Webber⁵³, D. Websdale⁵², M. Whitehead⁴⁷, J. Wicht³⁷, J. Wiechczynski²⁵, D. Wiedner¹¹, L. Wiggers⁴⁰, G. Wilkinson⁵⁴, M.P. Williams^{47,48}, M. Williams⁵⁵, F.F. Wilson⁴⁸, J. Wimberley⁵⁷, J. Wishahi⁹, W. Wislicki²⁷, M. Witek²⁵, G. Wormser⁷, S.A. Wotton⁴⁶, S. Wright⁴⁶, S. Wu³, K. Wyllie³⁷, Y. Xie^{49,37}, Z. Xing⁵⁸, Z. Yang³, X. Yuan³, O. Yushchenko³⁴, M. Zangoli¹⁴, M. Zavertyaev^{10,b}, F. Zhang³, L. Zhang⁵⁸, W.C. Zhang¹², Y. Zhang³, A. Zhelezov¹¹, A. Zhokhov³⁰, L. Zhong³, A. Zvyagin³⁷.

¹ *Centro Brasileiro de Pesquisas Físicas (CBPF), Rio de Janeiro, Brazil*

² *Universidade Federal do Rio de Janeiro (UFRJ), Rio de Janeiro, Brazil*

³ *Center for High Energy Physics, Tsinghua University, Beijing, China*

⁴ *LAPP, Université de Savoie, CNRS/IN2P3, Annecy-Le-Vieux, France*

⁵ *Clermont Université, Université Blaise Pascal, CNRS/IN2P3, LPC, Clermont-Ferrand, France*

⁶ *CPPM, Aix-Marseille Université, CNRS/IN2P3, Marseille, France*

⁷ *LAL, Université Paris-Sud, CNRS/IN2P3, Orsay, France*

⁸ *LPNHE, Université Pierre et Marie Curie, Université Paris Diderot, CNRS/IN2P3, Paris, France*

⁹ *Fakultät Physik, Technische Universität Dortmund, Dortmund, Germany*

¹⁰ *Max-Planck-Institut für Kernphysik (MPIK), Heidelberg, Germany*

¹¹ *Physikalisches Institut, Ruprecht-Karls-Universität Heidelberg, Heidelberg, Germany*

¹² *School of Physics, University College Dublin, Dublin, Ireland*

¹³ *Sezione INFN di Bari, Bari, Italy*

¹⁴ *Sezione INFN di Bologna, Bologna, Italy*

¹⁵ *Sezione INFN di Cagliari, Cagliari, Italy*

¹⁶ *Sezione INFN di Ferrara, Ferrara, Italy*

¹⁷ *Sezione INFN di Firenze, Firenze, Italy*

¹⁸ *Laboratori Nazionali dell'INFN di Frascati, Frascati, Italy*

¹⁹ *Sezione INFN di Genova, Genova, Italy*

²⁰ *Sezione INFN di Milano Bicocca, Milano, Italy*

²¹ *Sezione INFN di Padova, Padova, Italy*

²² *Sezione INFN di Pisa, Pisa, Italy*

²³ *Sezione INFN di Roma Tor Vergata, Roma, Italy*

²⁴ *Sezione INFN di Roma La Sapienza, Roma, Italy*

²⁵ *Henryk Niewodniczanski Institute of Nuclear Physics Polish Academy of Sciences, Kraków, Poland*

²⁶ *AGH - University of Science and Technology, Faculty of Physics and Applied Computer Science, Kraków, Poland*

- ²⁷ *National Center for Nuclear Research (NCBJ), Warsaw, Poland*
- ²⁸ *Horia Hulubei National Institute of Physics and Nuclear Engineering, Bucharest-Magurele, Romania*
- ²⁹ *Petersburg Nuclear Physics Institute (PNPI), Gatchina, Russia*
- ³⁰ *Institute of Theoretical and Experimental Physics (ITEP), Moscow, Russia*
- ³¹ *Institute of Nuclear Physics, Moscow State University (SINP MSU), Moscow, Russia*
- ³² *Institute for Nuclear Research of the Russian Academy of Sciences (INR RAN), Moscow, Russia*
- ³³ *Budker Institute of Nuclear Physics (SB RAS) and Novosibirsk State University, Novosibirsk, Russia*
- ³⁴ *Institute for High Energy Physics (IHEP), Protvino, Russia*
- ³⁵ *Universitat de Barcelona, Barcelona, Spain*
- ³⁶ *Universidad de Santiago de Compostela, Santiago de Compostela, Spain*
- ³⁷ *European Organization for Nuclear Research (CERN), Geneva, Switzerland*
- ³⁸ *Ecole Polytechnique Fédérale de Lausanne (EPFL), Lausanne, Switzerland*
- ³⁹ *Physik-Institut, Universität Zürich, Zürich, Switzerland*
- ⁴⁰ *Nikhef National Institute for Subatomic Physics, Amsterdam, The Netherlands*
- ⁴¹ *Nikhef National Institute for Subatomic Physics and VU University Amsterdam, Amsterdam, The Netherlands*
- ⁴² *NSC Kharkiv Institute of Physics and Technology (NSC KIPT), Kharkiv, Ukraine*
- ⁴³ *Institute for Nuclear Research of the National Academy of Sciences (KINR), Kyiv, Ukraine*
- ⁴⁴ *University of Birmingham, Birmingham, United Kingdom*
- ⁴⁵ *H.H. Wills Physics Laboratory, University of Bristol, Bristol, United Kingdom*
- ⁴⁶ *Cavendish Laboratory, University of Cambridge, Cambridge, United Kingdom*
- ⁴⁷ *Department of Physics, University of Warwick, Coventry, United Kingdom*
- ⁴⁸ *STFC Rutherford Appleton Laboratory, Didcot, United Kingdom*
- ⁴⁹ *School of Physics and Astronomy, University of Edinburgh, Edinburgh, United Kingdom*
- ⁵⁰ *School of Physics and Astronomy, University of Glasgow, Glasgow, United Kingdom*
- ⁵¹ *Oliver Lodge Laboratory, University of Liverpool, Liverpool, United Kingdom*
- ⁵² *Imperial College London, London, United Kingdom*
- ⁵³ *School of Physics and Astronomy, University of Manchester, Manchester, United Kingdom*
- ⁵⁴ *Department of Physics, University of Oxford, Oxford, United Kingdom*
- ⁵⁵ *Massachusetts Institute of Technology, Cambridge, MA, United States*
- ⁵⁶ *University of Cincinnati, Cincinnati, OH, United States*
- ⁵⁷ *University of Maryland, College Park, MD, United States*
- ⁵⁸ *Syracuse University, Syracuse, NY, United States*
- ⁵⁹ *Pontifícia Universidade Católica do Rio de Janeiro (PUC-Rio), Rio de Janeiro, Brazil, associated to ²*
- ⁶⁰ *Institut für Physik, Universität Rostock, Rostock, Germany, associated to ¹¹*
- ⁶¹ *National Research Centre Kurchatov Institute, Moscow, Russia, associated to ³⁰*
- ⁶² *KVI - University of Groningen, Groningen, The Netherlands, associated to ⁴⁰*
- ⁶³ *Celal Bayar University, Manisa, Turkey, associated to ³⁷*

^a *Universidade Federal do Triângulo Mineiro (UFMT), Uberaba-MG, Brazil*

^b *P.N. Lebedev Physical Institute, Russian Academy of Science (LPI RAS), Moscow, Russia*

^c *Università di Bari, Bari, Italy*

^d *Università di Bologna, Bologna, Italy*

^e *Università di Cagliari, Cagliari, Italy*

^f *Università di Ferrara, Ferrara, Italy*

^g *Università di Firenze, Firenze, Italy*

^h *Università di Urbino, Urbino, Italy*

ⁱ *Università di Modena e Reggio Emilia, Modena, Italy*

^j *Università di Genova, Genova, Italy*

^k *Università di Milano Bicocca, Milano, Italy*

^l *Università di Roma Tor Vergata, Roma, Italy*

^m *Università di Roma La Sapienza, Roma, Italy*

ⁿ *Università della Basilicata, Potenza, Italy*

^o *AGH - University of Science and Technology, Faculty of Computer Science, Electronics and Telecommunications, Kraków, Poland*

^p *LIFAELS, La Salle, Universitat Ramon Llull, Barcelona, Spain*

^q *Hanoi University of Science, Hanoi, Viet Nam*

^r *Università di Padova, Padova, Italy*

^s *Università di Pisa, Pisa, Italy*

^t *Scuola Normale Superiore, Pisa, Italy*

1 Introduction

The study of beauty baryon decays is still at an early stage. Among the possible ground states with spin-parity $J^P = \frac{1}{2}^+$ [1], no hadronic three-body decay to a charmless final state has been observed. These channels provide interesting possibilities to study hadronic decays and to search for CP violation effects, which may vary significantly across the phase-space [2,3], as recently observed in charged B meson decays to charmless three-body final states [4,5]. In contrast to three-body neutral B meson decays to charmless final states containing K_s^0 mesons [6], conservation of baryon number allows CP violation searches without the need to identify the flavour of the initial state.

In this paper, a search is presented for Λ_b^0 and Ξ_b^0 baryon decays to final states containing a K_s^0 meson, a proton and either a kaon or a pion (denoted $\Lambda_b^0(\Xi_b^0) \rightarrow K_s^0 p h^-$ where $h = \pi, K$).¹ No published theoretical prediction or experimental limit exists for their branching fractions. Intermediate states containing charmed hadrons are excluded from the signal sample and studied separately: the $\Lambda_b^0 \rightarrow \Lambda_c^+(\rightarrow p K_s^0)\pi^-$ decay is used as a control channel, while the $\Lambda_b^0 \rightarrow \Lambda_c^+(\rightarrow p K_s^0)K^-$ and $\Lambda_b^0 \rightarrow D_s^-(\rightarrow K_s^0 K^-)p$ decays are also searched for. The $\Lambda_b^0 \rightarrow \Lambda_c^+(\rightarrow p K^- \pi^+)K^-$ decay has recently been observed [7], while the $\Lambda_b^0 \rightarrow D_s^- p$ decay has been suggested as a source of background to the $B_s^0 \rightarrow D_s^\mp K^\pm$ mode [8]. All branching fractions are measured relative to that of the well-known control channel $B^0 \rightarrow K^0 \pi^+ \pi^-$ [6,9,10], relying on existing measurements of the ratio of fragmentation fractions $f_{\Lambda_b^0}/f_a$, including its transverse momentum (p_T) dependence [11–13]. When quoting absolute branching fractions, the results are expressed in terms of final states containing either K^0 or \bar{K}^0 mesons, according to the expectation for each decay, following the convention in the literature [1,14].

The paper is organised as follows. A brief description of the LHCb detector and the data set used for the analysis is given in Sec. 2. The selection algorithms, the method to determine signal yields, and the systematic uncertainties on the results are discussed in Secs. 3–5. The measured branching fractions are presented in Sec. 6. Since a significant signal is observed for the $\Lambda_b^0 \rightarrow K_s^0 p \pi^-$ channel, a measurement of its phase-space integrated CP asymmetry is reported in Sec. 7. Conclusions are given in Sec. 8.

2 Detector and data set

The LHCb detector [15] is a single-arm forward spectrometer covering the pseudorapidity range $2 < \eta < 5$, designed for the study of particles containing b or c quarks. The detector includes a high precision tracking system consisting of a silicon-strip vertex detector surrounding the pp interaction region, a large-area silicon-strip detector located upstream of a dipole magnet with a bending power of about 4 Tm, and three stations of silicon-strip detectors and straw drift tubes placed downstream. The combined tracking system provides momentum measurement with relative uncertainty that varies from 0.4%

¹ The inclusion of charge-conjugate processes is implied throughout this paper, except where asymmetries are discussed.

at 5 GeV/ c to 0.6% at 100 GeV/ c , and impact parameter (IP) resolution of 20 μm for tracks with high transverse momentum. Charged hadrons are identified using two ring-imaging Cherenkov (RICH) detectors [16]. Photon, electron and hadron candidates are identified by a calorimeter system consisting of scintillating-pad and preshower detectors, an electromagnetic calorimeter and a hadronic calorimeter. Muons are identified by a system composed of alternating layers of iron and multiwire proportional chambers [17]. The trigger [18] consists of a hardware stage, based on information from the calorimeter and muon systems, followed by a software stage, which applies a full event reconstruction.

The analysis is based on a sample, corresponding to an integrated luminosity of 1.0 fb^{-1} of pp collision data at a centre-of-mass energy of 7 TeV, collected with the LHCb detector during 2011. Samples of simulated events are also used to determine the signal selection efficiency, to model signal event distributions and to investigate possible background contributions. In the simulation, pp collisions are generated using PYTHIA 6.4 [19] with a specific LHCb configuration [20]. Decays of hadronic particles are described by EVTGEN [21], in which final-state radiation is generated using PHOTOS [22]. The interaction of the generated particles with the detector and its response are implemented using the GEANT4 toolkit [23] as described in Ref. [24].

3 Selection requirements, efficiency modelling and background studies

Events are triggered and subsequently selected in a similar way for both $\Lambda_b^0(\Xi_b^0) \rightarrow K_s^0 p h^-$ signal modes and the $B^0 \rightarrow K_s^0 \pi^+ \pi^-$ normalisation channel. Events are required to be triggered at hardware level either by a calorimeter signal with transverse energy $E_T > 3.5 \text{ GeV}$ associated with one of the particles in the signal decay chain, or by a particle in the event that is independent of the signal decay. The software trigger requires a two-, three- or four-track secondary vertex with a large sum of the transverse momentum of the tracks and significant displacement from the primary pp interaction vertices (PVs). At least one track should have $p_T > 1.7 \text{ GeV}/c$ and χ_{IP}^2 with respect to any PV greater than 16, where χ_{IP}^2 is defined as the difference in χ^2 of a given PV reconstructed with and without the considered particle. A multivariate algorithm [25] is used for the identification of secondary vertices consistent with the decay of a b hadron.

An initial set of loose requirements is applied to filter the events selected by the trigger. Each b hadron (Λ_b^0 , Ξ_b^0 or B^0) decay is reconstructed by combining two charged tracks with a K_s^0 candidate. The K_s^0 candidates are reconstructed in the $\pi^+ \pi^-$ final state, and are classified into two categories. The first includes candidates that have hits in the vertex detector and the tracking stations downstream of the dipole magnet, hereafter referred to as ‘‘Long’’. The second category includes those decays in which track segments for the two pions are not found in the vertex detector, and use only the tracking stations downstream of the vertex detector (‘‘Downstream’’). The pions are required to have momentum $p > 2 \text{ GeV}/c$ and to form a vertex with $\chi_{\text{vtx}}^2 < 12$. In addition, for Downstream (Long) K_s^0 type the pions must have minimum χ_{IP}^2 with respect to any PV greater than

4 (9), and the pair must satisfy $|m(\pi^+\pi^-) - m_{K_s^0}| < 30$ (20) MeV/c^2 , where $m_{K_s^0}$ is the known K_s^0 mass [1]. The K_s^0 candidate is associated to the PV that minimises the χ_{IP}^2 , and the square of the separation distance between the K_s^0 vertex and the associated PV divided by its uncertainty (χ_{VS}^2), must be greater than 50 (90) for Downstream (Long) candidates. For Downstream K_s^0 candidates $p > 6$ GeV/c is also required.

For both signal modes and the normalisation channel, the selection exploits the topology of the three-body decay and the b hadron kinematic properties. The scalar sum of the transverse momenta of the daughters is required to be greater than 3 GeV/c and at least two of the daughters must have $p_{\text{T}} > 0.8$ GeV/c . The IP of the charged daughter with the largest p_{T} is required to be greater than 0.05 mm. The minimum for each pair of two daughters of the square of the distance of closest approach divided by its uncertainty must be less than 5. Furthermore, it is required that the b hadron candidate has $\chi_{\text{vtx}}^2 < 12$, $\chi_{\text{IP}}^2 < 4$, $\chi_{\text{VS}}^2 > 50$, that its vertex separation from the PV must be greater than 1 mm, that the cosine of the “pointing” angle between its momentum vector and the line joining its production and decay vertices must be greater than 0.9999, and that it has $p_{\text{T}} > 1.5$ GeV/c . Additional requirements are imposed to reduce background: the separation between the K_s^0 and b hadron candidate vertices must be positive in the z direction;² and the K_s^0 flight distance must be greater than 15 mm. The b hadron candidates are required to have invariant mass within the ranges $5469 < m(K_s^0 p h^-) < 5938$ MeV/c^2 , evaluated for both $h = K, \pi$ hypotheses, and $4779 < m(K_s^0 \pi^+ \pi^-) < 5866$ MeV/c^2 . To avoid potential biases during the selection optimisation, regions of ± 50 MeV/c^2 (*cf.* the typical resolution of 15 MeV/c^2) around both the Λ_b^0 and Ξ_b^0 known masses were not examined until the selection criteria were established.

Further separation of signal from combinatorial background candidates is achieved with a boosted decision tree (BDT) multivariate classifier [26, 27]. The BDT is trained using the $B^0 \rightarrow K_s^0 \pi^+ \pi^-$ control channel as a proxy for the signal decays, with simulated samples used for the signal and data from the sideband region $5420 < m(K_s^0 \pi^+ \pi^-) < 5866$ MeV/c^2 for the background. Potential baryonic contributions in the sidebands from $\Lambda_b^0 \rightarrow K_s^0 p \pi^-$ and $\Lambda_c^+ \rightarrow K_s^0 p$ decays are reduced by vetoing the relevant invariant masses in appropriate ranges. In order to avoid bias in the training, the sample is split randomly into two, and two separate BDT trainings are used. The set of input variables is chosen to optimise the performance of the algorithm, and to minimise efficiency variation across the phase-space. The input variables for the BDTs are the p_{T} , η , χ_{IP}^2 , χ_{VS}^2 , pointing angle and χ_{vtx}^2 of the b hadron candidate; the sum of the χ_{IP}^2 values of the h^+ and h^- tracks (here $h = \pi, K, p$); and the χ_{IP}^2 , χ_{VS}^2 and χ_{vtx}^2 of the K_s^0 candidate.

The choice of the optimal BDT cut value is determined separately for each K_s^0 category, and separately for the charmless signal modes and for the channels containing intermediate Λ_c^+ or D_s^- hadrons. An appropriate figure of merit for previously unobserved modes is [28],

$$Q = \frac{\epsilon_{\text{sig}}}{a/2 + \sqrt{B}}, \quad (1)$$

where $a = 5$ quantifies the target level of significance in units of standard deviations, ϵ_{sig} is

²The z axis points along the beam line from the interaction region through the LHCb detector.

the efficiency of the signal selection determined from the simulation, and B is the expected number of background events in the signal region, which is estimated by extrapolating the result of a fit to the invariant mass distribution of the data sidebands. An alternative optimisation approach, which minimises the expected upper limit [29], is also investigated and provides a similar result.

Potential sources of remaining background are suppressed with particle identification (PID) criteria. This is of particular importance for reducing cross feed between the signal channels due to kaon/pion misidentification. Particle identification information is provided by the RICH detectors [16], in terms of the logarithm of the likelihood ratio between the kaon/proton and pion hypotheses ($DLL_{K\pi}$ and $DLL_{p\pi}$). A tight $DLL_{p\pi}$ criterion on the proton candidate suppresses most possible backgrounds from misidentified b hadron decays. An additional $DLL_{K\pi}$ requirement is imposed to reduce cross feed between $K_s^0 p \pi^-$ and $K_s^0 p K^-$ modes. In addition, candidates containing tracks with associated hits in the muon detectors are rejected. The DLL requirements are optimised using Eq. (1), and their efficiencies are determined using high-purity data control samples of $\Lambda \rightarrow p \pi^-$ and $D^0 \rightarrow K^- \pi^+$ decays, reweighted according to the expected signal kinematic (momentum and p_T) distributions from the simulation.

The efficiency of the selection requirements is studied with simulation. A multibody decay can in general proceed through intermediate states and through a nonresonant amplitude. It is therefore necessary to model the variation of the efficiency, and to account for the distribution of signal events, over the phase-space of the decay. The phase-space of the decay of a spin-zero particle to three spin-zero particles can be completely described by the Dalitz plot [30] of any pair of the two-body invariant masses squared. The situation for a baryon decay is more complicated due to the spins of the initial and final state fermions, but the conventional Dalitz plot can still be used if spin effects are neglected.³ For three-body b hadron decays, both signal decays and the dominant combinatorial backgrounds populate regions close to the kinematic boundaries of the conventional Dalitz plot. For more accurate modelling of those regions, it is convenient to transform to a rectangular space (hereafter referred to as the square Dalitz plot [32]) described by the variables m' and θ' where

$$m' \equiv \frac{1}{\pi} \arccos \left(2 \frac{m(K_s^0 p) - m^{\min}(K_s^0 p)}{m^{\max}(K_s^0 p) - m^{\min}(K_s^0 p)} - 1 \right), \quad \theta' \equiv \frac{1}{\pi} \theta(K_s^0 p). \quad (2)$$

Here $m(K_s^0 p)$ is the invariant mass of the K_s^0 and proton, $m^{\max}(K_s^0 p) = m_{\Lambda_b^0} - m_{h^-}$ and $m^{\min}(K_s^0 p) = m_{K_s^0} + m_p$ are the boundaries of $m(K_s^0 p)$, $\theta(K_s^0 p)$ is the angle between the p and the h^- track in the $K_s^0 p$ rest frame.

Simulated events are binned in the square Dalitz plot variables in order to determine the selection efficiencies. If no significant b hadron signal is seen, the efficiency corresponding to a uniform distribution across the square Dalitz plot is used as the nominal value, and a systematic uncertainty is assigned due to the variation across the phase-space. When the

³ Note that Λ_b^0 baryons produced in pp collisions at $\sqrt{s} = 7$ TeV have been measured to have only a small degree of polarisation [31].

signal yield has significance (evaluated as described in the next section) greater than 3σ , the signal distribution in the square Dalitz plot is obtained with the *sPlot* technique [33] (with the b hadron candidate invariant mass used as the control variable), and the efficiency corresponding to the observed distribution is used.

There is limited prior knowledge of the branching fractions of b baryon decays that may form backgrounds to the current search. Numerous modes are investigated with simulation, and the only significant potential background contribution that is found to peak in the candidate mass distribution is from $\Lambda_b^0 \rightarrow \Lambda_c^+(\rightarrow pK^-\pi^+)h^-$ decays, where the kaon is misidentified as a pion, and the πK pair can form a K_s^0 candidate. To suppress this background, candidates that have $pK^-\pi^+$ masses within $30 \text{ MeV}/c^2$ of the known Λ_c^+ mass are vetoed.

The decays $\Lambda_b^0 \rightarrow \Lambda_c^+(\rightarrow pK_s^0)h^-$ and $\Lambda_b^0 \rightarrow D_s^-(\rightarrow K_s^0 K^-)p$ share the same final state as the charmless signal modes and are removed by vetoing regions in $m(K_s^0 p)$ and $m(K_s^0 K)$ within $\pm 30 \text{ MeV}/c^2$ of the known Λ_c^+ and D_s^- masses. These vetoes are reversed to select and study the decay modes with intermediate charmed states. The additional requirement for the charmed modes reduces the combinatorial background. Therefore the optimal BDT requirement is obtained separately for each channel.

The backgrounds to the normalisation channel are treated as in Ref. [6]. The main contributions are considered to be charmless decays with an unreconstructed photon in the final state (*e.g.* $B^0 \rightarrow K_s^0 \pi^+ \pi^- \gamma$ or $B^0 \rightarrow \eta'(\rightarrow \rho^0 \gamma)K_s^0$), charmless decays of B^0 or B^+ mesons into two vector particles (*e.g.* $B^0 \rightarrow K^{*0}(\rightarrow K_s^0 \pi^0)\rho^0$ and $B^+ \rightarrow K^{*+}(\rightarrow K_s^0 \pi^+)\rho^0$) where a soft pion is not reconstructed, and charmed decays (*e.g.* $B^- \rightarrow D^0(\rightarrow K_s^0 \pi^+ \pi^-)\pi^-$) where a pion is not reconstructed.

4 Fit model and results

All signal and background yields are determined simultaneously by performing an unbinned extended maximum likelihood fit to the b hadron candidate invariant mass distribution of each final state and K_s^0 category. The probability density function (PDF) in each invariant mass distribution is defined as the sum of several components (signal, cross-feed contributions, combinatorial and other backgrounds), with shapes derived from simulation.

Signal PDFs are known to have asymmetric tails that result from a combination of the effects of final state radiation and stochastic tracking imperfections. The $\Lambda_b^0(\Xi_b^0) \rightarrow K_s^0 p h^-$ signal mass distributions are modelled by the sum of a “core” Gaussian and a bifurcated Gaussian function, that share the same mean value. The core resolution is allowed to be different for each K_s^0 category, whilst the two widths of the bifurcated Gaussian are common to Downstream and Long types. Alternative shapes are studied using simulation, and this choice is found to provide the most stable and accurate description for a given number of parameters.

The significant yield of $\Lambda_b^0 \rightarrow \Lambda_c^+(\rightarrow pK_s^0)\pi^-$ decays allows a subset of fit parameters common to the unobserved b baryon decays to be determined from data. The core width and the relative fraction between the Gaussian and bifurcated Gaussian component are

therefore expressed in terms of the parameters obtained from the fit to $\Lambda_b^0 \rightarrow \Lambda_c^+(\rightarrow pK_s^0)\pi^-$ candidates, with deviations from those values allowed within ranges as seen in the simulation. Explicitly, the function used for each unobserved channel j and K_s^0 type c is

$$\text{PDF}(m; \mu, \sigma_{\text{core}}^c, \sigma_{\text{R}}, \sigma_{\text{L}}) = s_f^{c,j} f^c G(m; \mu, s_\sigma^{c,j} \sigma_{\text{core}}^c) + (1 - s_f^{c,j} f^c) B(m; \mu, \sigma_{\text{L}}, \sigma_{\text{R}}), \quad (3)$$

where m is the invariant mass of the b hadron candidate and G and B represent the Gaussian and bifurcated Gaussian distributions respectively. The parameters σ_{L} and σ_{R} are respectively the left and right widths of the bifurcated Gaussian function, σ_{core}^c and f^c are the width and the fraction of the core Gaussian for $\Lambda_b^0 \rightarrow \Lambda_c^+(\rightarrow pK_s^0)\pi^-$ candidates, while $s_\sigma^{c,j}$ and $s_f^{c,j}$ are the corresponding scale factors for the channel j , determined from simulation. The peak position μ for Λ_b^0 decays is shared among all modes, while that for Ξ_b^0 decays is fixed according to the measured Λ_b^0 and Ξ_b^0 mass difference, $m_{\Xi_b^0} - m_{\Lambda_b^0} = 168.6 \pm 5.0 \text{ MeV}/c^2$ [1]. The scale factors for Λ_b^0 and Ξ_b^0 signal shapes are allowed to differ but are found to be consistent. The fit model and its stability are validated with ensembles of pseudo-experiments, and no significant bias is found.

The normalisation channel is parametrised following Ref. [6]. The signal distribution of the B candidate invariant mass is modelled by the sum of two Crystal Ball (CB) functions [34], where the power law tails are on opposite sides of the peak. The two CB functions are constrained to have the same peak position and resolution, which are floated in the fit. The tail parameters and the relative normalisation of the two CB functions are taken from the simulation and fixed in the fit to data. To account for $B_s^0 \rightarrow K_s^0 \pi^+ \pi^-$ decays [6] an additional component, parametrised in the same way as the B^0 channel, is included. Its peak position is fixed according to the known $B_s^0 - B^0$ mass difference [1], its width is constrained to be the same as that seen for the B^0 mode to within the difference found in simulation, and its yield is allowed to vary independently.

An exponential shape is used to describe the combinatorial background, which is treated as independent for each decay mode and K_s^0 type. Cross-feed contributions are also considered for each $K_s^0 p h^-$ final state. For the normalisation channel, a contribution from $B_s^0 \rightarrow K_s^0 K^\pm \pi^\mp$ decays is included, while yields of other possible misidentified backgrounds are found to be negligible [6]. Cross-feed and misidentified $B_s^0 \rightarrow K_s^0 K^\pm \pi^\mp$ shapes are modelled by double CB functions, with independent peak positions and resolutions. The yields of these components are constrained to be consistent with the number of signal candidates in the corresponding correctly identified spectrum, multiplied by the relevant misidentification probability. The peaking backgrounds to the normalisation channel reported in Sec. 3 are modelled by a generalised ARGUS function [35] convolved with a Gaussian function with width determined from simulation. The yield of each contribution is constrained within uncertainty according to the corresponding efficiency and branching fraction.

The results of the fit to data are shown in Fig. 1 for $\Lambda_b^0(\Xi_b^0) \rightarrow K_s^0 p h^-$ candidates, Fig. 2 for $\Lambda_b^0 \rightarrow \Lambda_c^+(\rightarrow pK_s^0)h^-$ and $\Lambda_b^0 \rightarrow D_s^- p$ candidates and Fig. 3 for the $B^0 \rightarrow K_s^0 \pi^+ \pi^-$ normalisation channel, separated by K_s^0 type. The fitted yields and relevant efficiencies are gathered in Table 1. The statistical significance of each signal is computed as $\sqrt{2 \ln(L_{\text{sig}}/L_0)}$, where L_{sig} and L_0 are the likelihoods from the nominal fit and from

the fit omitting the signal component, respectively. These statistical likelihood curves for each K_s^0 category are convolved with a Gaussian function of width given by the systematic uncertainty on the fit yield. The total significance, for Downstream and Long K_s^0 types combined, is found to be 8.6σ and 2.1σ for $\Lambda_b^0 \rightarrow K_s^0 p \pi^-$ and $\Lambda_b^0 \rightarrow K_s^0 p K^-$ decays, respectively. Moreover, the statistical significance for the $\Lambda_b^0 \rightarrow \Lambda_c^+ (\rightarrow p K_s^0) K^-$ decay is found to be 9.4σ and 8.0σ for Downstream and Long categories respectively, confirming the recent observation of this channel [7]. The significances of all other channels are below 2σ .

The Dalitz plot distribution of $\Lambda_b^0 \rightarrow K_s^0 p \pi^-$ decays, shown in Fig. 4, is obtained using the *sPlot* technique and applying event-by-event efficiency corrections based on the position of the decay in the square Dalitz plot. A structure at low $p\pi^-$ invariant mass, which may originate from excited nucleon states, is apparent but there are no clear structures in the other two invariant mass combinations.

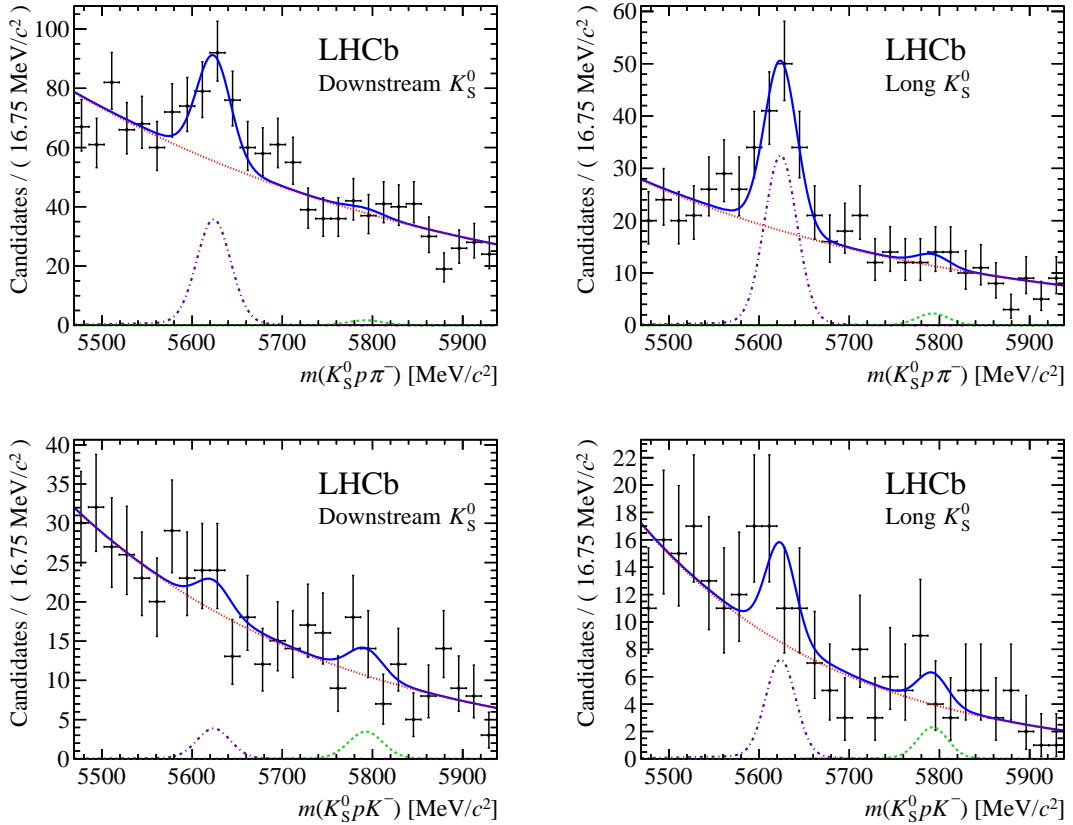


Figure 1: Invariant mass distribution of (top) $K_s^0 p \pi^-$ and (bottom) $K_s^0 p K^-$ candidates for the (left) Downstream and (right) Long K_s^0 categories after the final selection in the full data sample. Each significant component of the fit model is displayed: Λ_b^0 signal (violet dot-dashed), Ξ_b^0 signal (green dashed) and combinatorial background (red dotted). The overall fit is given by the solid blue line. Contributions with very small yields are not shown.

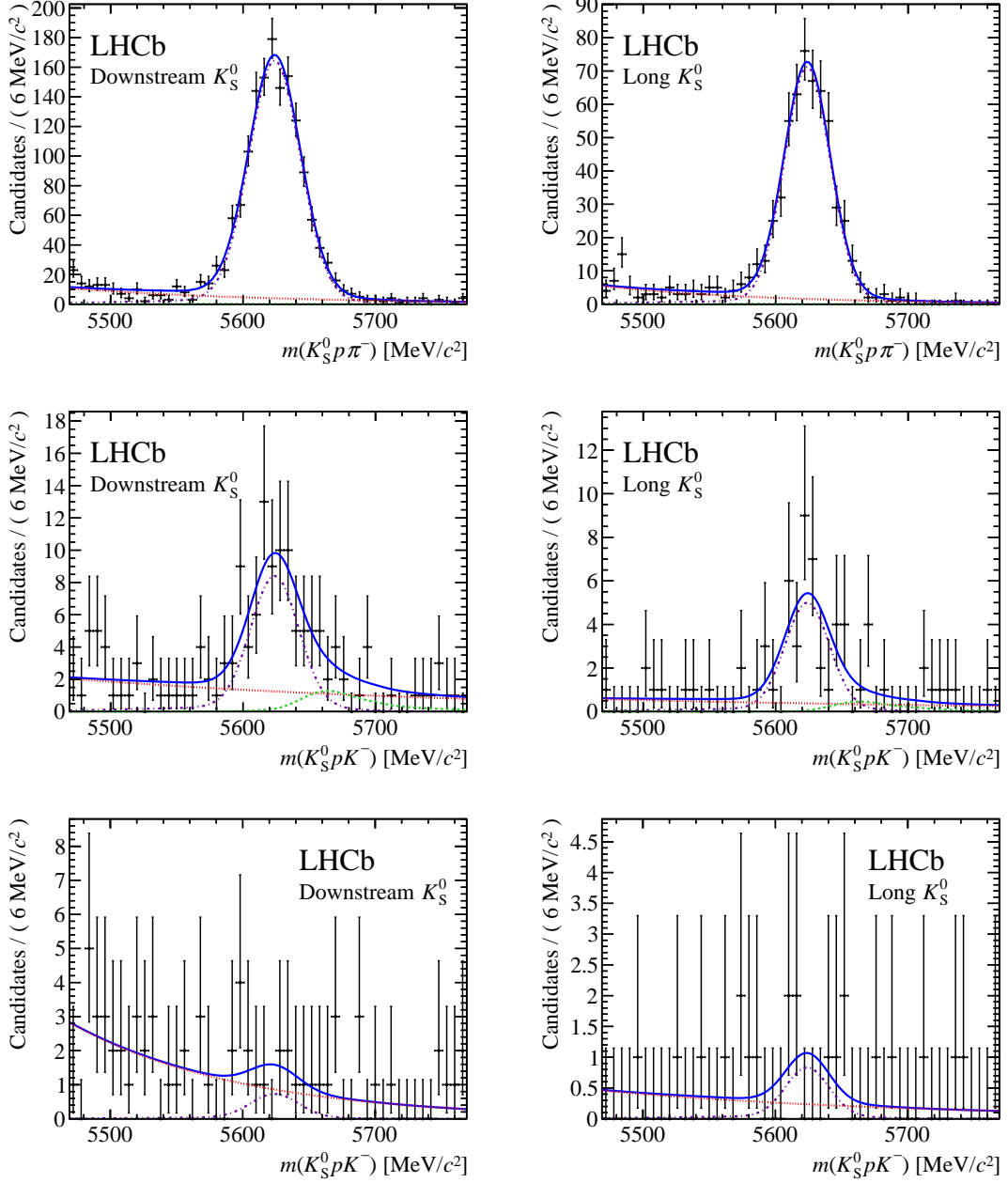


Figure 2: Invariant mass distribution of (top) $\Lambda_b^0 \rightarrow \Lambda_c^+ (\rightarrow p K_S^0) \pi^-$, (middle) $\Lambda_b^0 \rightarrow \Lambda_c^+ (\rightarrow p K_S^0) K^-$ and (bottom) $\Lambda_b^0 \rightarrow D_s^- (\rightarrow K_S^0 K^-) p$ candidates for the (left) Downstream and (right) Long K_S^0 categories after the final selection in the full data sample. Each significant component of the fit model is displayed: signal PDFs (violet dot-dashed), signal cross-feed contributions (green dashed) and combinatorial background (red dotted). The overall fit is given by the solid blue line. Contributions with very small yields are not shown.

Table 1: Fitted yields and efficiency for each channel, separated by K_s^0 type. Yields are given with both statistical and systematic uncertainties, whereas for the efficiencies only the uncertainties due to the limited Monte Carlo sample sizes are given. The three rows for the $B^0 \rightarrow K_s^0 \pi^+ \pi^-$ decay correspond to the different BDT selections for charmless signal modes and the channels containing Λ_c^+ or D_s^- hadrons.

Mode	Downstream		Long	
	Yield	Efficiency ($\times 10^{-4}$)	Yield	Efficiency ($\times 10^{-4}$)
$\Lambda_b^0 \rightarrow K_s^0 p \pi^-$	$106.1 \pm 21.5 \pm 3.7$	5.40 ± 0.12	$90.9 \pm 14.6 \pm 1.0$	2.26 ± 0.06
$\Lambda_b^0 \rightarrow K_s^0 p K^-$	$11.5 \pm 10.7 \pm 1.2$	5.34 ± 0.11	$19.6 \pm 8.5 \pm 0.8$	2.87 ± 0.07
$\Xi_b^0 \rightarrow K_s^0 p \pi^-$	$5.3 \pm 15.7 \pm 0.7$	5.35 ± 0.10	$6.4 \pm 8.5 \pm 0.5$	2.67 ± 0.07
$\Xi_b^0 \rightarrow K_s^0 p K^-$	$10.5 \pm 8.8 \pm 0.5$	6.12 ± 0.10	$6.3 \pm 5.6 \pm 0.4$	2.91 ± 0.07
$\Lambda_b^0 \rightarrow \Lambda_c^+ (\rightarrow p K_s^0) \pi^-$	$1391.6 \pm 39.6 \pm 24.8$	4.85 ± 0.09	$536.8 \pm 24.6 \pm 3.5$	1.71 ± 0.05
$\Lambda_b^0 \rightarrow \Lambda_c^+ (\rightarrow p K_s^0) K^-$	$70.0 \pm 10.3 \pm 3.3$	4.69 ± 0.07	$37.4 \pm 7.1 \pm 2.7$	1.66 ± 0.03
$\Lambda_b^0 \rightarrow D_s^- p$	$6.3 \pm 5.1 \pm 0.6$	2.69 ± 0.05	$6.5 \pm 3.7 \pm 0.2$	0.89 ± 0.03
$B^0 \rightarrow K_s^0 \pi^+ \pi^- (K_s^0 p h)$	$913.5 \pm 45.0 \pm 12.2$	5.57 ± 0.09	$495.7 \pm 31.8 \pm 7.5$	2.86 ± 0.06
$B^0 \rightarrow K_s^0 \pi^+ \pi^- (\Lambda_c^+ h)$	$1163.8 \pm 60.7 \pm 18.8$	7.38 ± 0.11	$589.0 \pm 33.3 \pm 17.3$	3.27 ± 0.06
$B^0 \rightarrow K_s^0 \pi^+ \pi^- (D_s^- p)$	$1317.8 \pm 77.1 \pm 25.7$	7.76 ± 0.11	$614.1 \pm 38.3 \pm 14.8$	3.47 ± 0.07

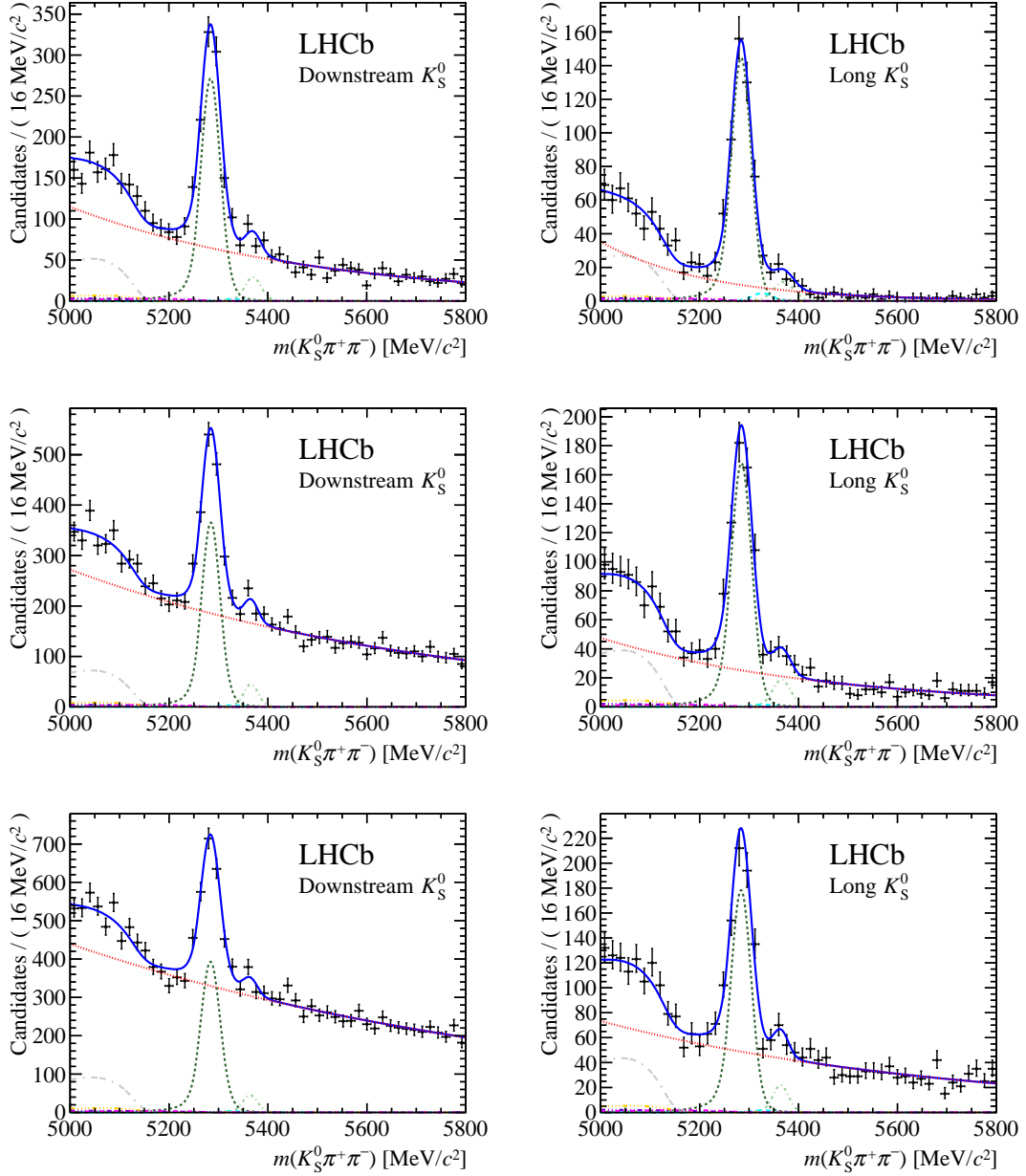


Figure 3: Invariant mass distribution of $K_S^0 \pi^+ \pi^-$ candidates with the selection requirements for the (top) $\Lambda_b^0 \rightarrow K_S^0 p h^-$, (middle) $\Lambda_b^0 \rightarrow \Lambda_c^+ (\rightarrow p K_S^0) h^-$ and (bottom) $\Lambda_b^0 \rightarrow D_s^- p$ channels separated into (left) Downstream and (right) Long K_S^0 categories. Each component of the fit model is displayed: the B^0 (B_s^0) decay is represented by the dashed dark (dot dashed light) green line; the background from $B_s^0 \rightarrow K_S^0 K^\pm \pi^\mp$ decays by the long dashed cyan line; $B^- \rightarrow D^0 (\rightarrow K_S^0 \pi^+ \pi^-) \pi^-$ (grey double-dash dotted), charmless B^0 (B^+) decays (orange dash quadruple-dotted), $B^0 \rightarrow \eta' (\rho^0 \gamma) K_S^0$ (magenta dash double-dotted) and $B^0 \rightarrow K_S^0 \pi^+ \pi^- \gamma$ (dark violet dash triple-dotted) backgrounds; the overall fit is given by the solid blue line; and the combinatorial background by the dotted red line.

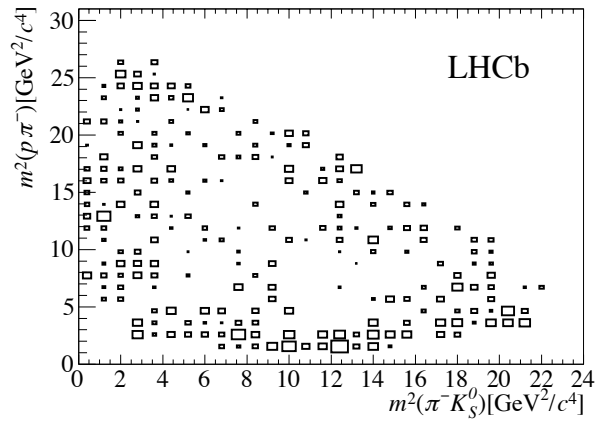


Figure 4: Background-subtracted, efficiency-corrected Dalitz plot distribution of $\Lambda_b^0 \rightarrow K_s^0 p \pi^-$ decays for Downstream and Long K_s^0 categories combined. Some bins have negative entries (consistent with zero) and appear empty.

5 Systematic uncertainties

The choice of normalisation channel is designed to minimise systematic uncertainties in the branching fraction determination. Since no b baryon decay has been previously measured with sufficient precision to serve as a normalisation channel, the $B^0 \rightarrow K_s^0 \pi^+ \pi^-$ channel is used. The remaining systematic uncertainties are summarised in Table 2 separately for each signal mode and K_s^0 type.

The efficiency determination procedures rely on the accuracy of the simulation. Uncertainties on the efficiencies arise due to the limited size of the simulation samples, differences between data and the simulation and, for the three-body modes, the variation of the efficiency over the phase-space.

The selection algorithms exploit the difference between signal and background in several variables. For the p_T and decay length variables, the distributions in data and simulation are known to differ, which can lead to a bias in the estimated efficiency. The p_T distribution for $\Lambda_b^0 \rightarrow \Lambda_c^+ \pi^-$ decays in data is obtained with the *sPlot* technique, and compared to that in the simulation. The corresponding possible bias in the efficiency is assigned as systematic uncertainty to each decay. The value of the Λ_b^0 lifetime used in the simulation differs from the most recent measurement [36]. A similar reweighting of the efficiency as done for the p_T distribution results in an estimate of the associated systematic uncertainty for the Λ_b^0 modes. The Ξ_b^0 lifetime is not yet measured, and no uncertainty is assigned to the value used in the simulation (1.42 ps) – unless the true lifetime is dramatically different from this value, the corresponding bias will in any case be negligible compared to other uncertainties. The uncertainties due to simulation, including also the small effect of limited simulation samples sizes, are combined in quadrature and

Table 2: Relative systematic uncertainties on the branching fraction ratios (%) with respect to $B^0 \rightarrow K_s^0 \pi^+ \pi^-$ decays. The total is obtained from the sum in quadrature of all contributions except that from knowledge of the fragmentation fractions.

Downstream	Simulation	Δ_{PHSP}	PID	Fit model	Fit bias	Vetoos	Total	$f_{\Lambda_b^0}/f_d$
$\mathcal{B}(\Lambda_b^0 \rightarrow K_s^0 p \pi^-)$	6	4	6	1	<1	3	10	27
$\mathcal{B}(\Lambda_b^0 \rightarrow K_s^0 p K^-)$	6	58	2	8	4	4	59	27
$\mathcal{B}(\Xi_b^0 \rightarrow K_s^0 p \pi^-)$	4	64	6	12	7	–	66	–
$\mathcal{B}(\Xi_b^0 \rightarrow K_s^0 p K^-)$	4	47	2	4	3	–	47	–
$\mathcal{B}(\Lambda_b^0 \rightarrow \Lambda_c^+ (\rightarrow p K_s^0) \pi^-)$	5	–	6	2	<1	<1	8	27
$\mathcal{B}(\Lambda_b^0 \rightarrow \Lambda_c^+ (\rightarrow p K_s^0) K^-)$	5	–	4	5	<1	1	8	27
$\mathcal{B}(\Lambda_b^0 \rightarrow D_s^- (\rightarrow K_s^0 K^-) p)$	6	–	6	7	6	–	12	27
Long								
$\mathcal{B}(\Lambda_b^0 \rightarrow K_s^0 p \pi^-)$	6	3	4	2	1	<1	8	27
$\mathcal{B}(\Lambda_b^0 \rightarrow K_s^0 p K^-)$	6	42	4	4	1	1	43	27
$\mathcal{B}(\Xi_b^0 \rightarrow K_s^0 p \pi^-)$	5	47	5	8	2	–	49	–
$\mathcal{B}(\Xi_b^0 \rightarrow K_s^0 p K^-)$	5	37	5	6	4	–	39	–
$\mathcal{B}(\Lambda_b^0 \rightarrow \Lambda_c^+ (\rightarrow p K_s^0) \pi^-)$	6	–	4	3	<1	<1	8	27
$\mathcal{B}(\Lambda_b^0 \rightarrow \Lambda_c^+ (\rightarrow p K_s^0) K^-)$	5	–	6	8	1	<1	11	27
$\mathcal{B}(\Lambda_b^0 \rightarrow D_s^- (\rightarrow K_s^0 K^-) p)$	6	–	8	4	2	–	11	27

listed as a single contribution in Table 2.

For modes without significant signals, the effect of efficiency variation across the phase-space (labelled Δ_{PHSP} in Table 2) is evaluated from the spread of the per-bin efficiency after dividing the square Dalitz plot in a coarse binning scheme. The large systematic uncertainties reflect the unknown distribution of signal events across the phase-space and the large efficiency variation. Conversely, the uncertainties on the normalisation and $\Lambda_b^0 \rightarrow K_s^0 p \pi^-$ channels are estimated by varying the square Dalitz plot binning scheme. For the $B^0 \rightarrow K_s^0 \pi^+ \pi^-$ mode the variation is found to be negligible. This source of uncertainty does not affect channels with intermediate charmed states, which have known distributions in the phase-space.

The particle identification efficiency and the contamination effects from signal cross-feed contributions are determined with a data-driven method as described in Sec. 3. In order to estimate possible systematic uncertainties inherent to this procedure, the method is re-evaluated with simulated samples of the control channels. These average efficiencies are compared to the efficiencies determined from the calibration samples and the differences are taken as estimates of the corresponding systematic uncertainty. The limited sizes of samples used in the PID calibration also contribute to the systematic uncertainty.

Alternative parametrisations are considered in order to verify the accuracy of the fit model and to assign a systematic uncertainty. The PDFs of the signal and normalisation channel are replaced respectively with a double CB and the sum of a Gaussian and a bifurcated Gaussian function, while the background model is changed to a second-order polynomial function. The systematic uncertainties are determined from pseudo-experiments, which are fitted with both nominal and alternative models. Pseudo-experiments are also used to investigate possible biases induced by the fit model; no significant biases are found, and uncertainties are assigned according to the size of the ensemble. Finally, the effects of the vetoes applied to remove charmed intermediate states are investigated by studying the variation in the result with different choices of requirements. The total systematic uncertainty is determined as the sum in quadrature of all contributions.

The fragmentation fraction of Λ_b^0 baryons ($f_{\Lambda_b^0}$) with respect to those of B^+ and B^0 mesons (f_u and f_d , respectively) has been measured by LHCb [11] to be

$$f_{\Lambda_b^0}/(f_u + f_d) = (0.404 \pm 0.110) \times [1 - (0.031 \pm 0.005) \times p_T(\text{GeV}/c)], \quad (4)$$

where the statistical, systematic and $\mathcal{B}(\Lambda_c^+ \rightarrow p K^- \pi^+)$ uncertainties are summed in quadrature, and the linear dependence is found to apply up to $p_T = 14 \text{ GeV}/c$. In the case of Ξ_b^0 baryons, there is no measurement of the fragmentation fraction, and therefore the results quoted include this factor.

The p_T dependence of the fragmentation fraction ratio given in Eq. (4) is obtained using semileptonic decays, and therefore is given in terms of the combined p_T of the charmed hadron and the muon in the final state. A correction due to the undetected neutrino is obtained from simulation, so that the appropriate fragmentation fraction ratio corresponding to the mean p_T for each signal mode can be determined ($f_u = f_d$ is assumed) [37]. For channels with significant signal the mean p_T is determined from data with the *sPlot* technique; otherwise the value from reconstructed simulated events is used.

Systematic uncertainties arise due to the parametrisation of $f_{\Lambda_b^0}/f_d$ versus p_T and possible inaccuracy in the mean p_T determination. This results in a fragmentation fraction of $f_{\Lambda_b^0}/f_d = 0.623 \pm 0.030, 0.590 \pm 0.031, 0.630 \pm 0.030, 0.628 \pm 0.030$ and 0.616 ± 0.030 for $\Lambda_b^0 \rightarrow K_s^0 p \pi^-$, $\Lambda_b^0 \rightarrow K_s^0 p K^-$, $\Lambda_b^0 \rightarrow \Lambda_c^+(\rightarrow p K_s^0) \pi^-$, $\Lambda_b^0 \rightarrow \Lambda_c^+(\rightarrow p K_s^0) K^-$ and $\Lambda_b^0 \rightarrow D_s^- p$ decays, respectively. The large uncertainty due to $\mathcal{B}(\Lambda_c^+ \rightarrow p K^- \pi^+)$ is not included in these values, but is accounted for separately.

6 Branching fraction results

The relative branching fractions are determined according to

$$\frac{\mathcal{B}(\Lambda_b^0(\Xi_b^0) \rightarrow K_s^0 p h^-)}{\mathcal{B}(B^0 \rightarrow K_s^0 \pi^+ \pi^-)} = \frac{\epsilon_{B^0 \rightarrow K_s^0 \pi^+ \pi^-}^{\text{sel}}}{\epsilon_{\Lambda_b^0(\Xi_b^0) \rightarrow K_s^0 p h^-}^{\text{sel}}} \times \frac{\epsilon_{B^0 \rightarrow K_s^0 \pi^+ \pi^-}^{\text{PID}}}{\epsilon_{\Lambda_b^0(\Xi_b^0) \rightarrow K_s^0 p h^-}^{\text{PID}}} \times \frac{N_{\Lambda_b^0(\Xi_b^0) \rightarrow K_s^0 p h^-}}{N_{B^0 \rightarrow K_s^0 \pi^+ \pi^-}} \times \frac{f_d}{f_{\Lambda_b^0(\Xi_b^0)}}, \quad (5)$$

where ϵ^{sel} and ϵ^{PID} are respectively the selection efficiency (which includes acceptance, reconstruction, offline selection and trigger components) and the particle identification efficiency, N is the signal yield and f is the fragmentation fraction. Each of these factors is determined separately for each decay and K_s^0 category. Each pair of results, for Downstream and Long K_s^0 types, is combined in a weighted average, where correlations in the systematic uncertainties are taken into account. For each mode, the results in the two K_s^0 categories agree within two standard deviations. For modes with significance below 3σ , upper limits are placed at both 90% and 95% confidence level (CL) by integrating the likelihood multiplied by a Bayesian prior that is uniform in the region of positive branching fraction.

The following relative branching fraction measurements and limits are obtained

$$\begin{aligned}
\frac{\mathcal{B}(\Lambda_b^0 \rightarrow K_s^0 p \pi^-)}{\mathcal{B}(B \rightarrow K_s^0 \pi^+ \pi^-)} &= 0.25 \pm 0.04 \text{ (stat)} \pm 0.02 \text{ (syst)} \pm 0.07 (f_{\Lambda_b^0}/f_d), \\
\frac{\mathcal{B}(\Lambda_b^0 \rightarrow K_s^0 p K^-)}{\mathcal{B}(B \rightarrow K_s^0 \pi^+ \pi^-)} &= 0.04 \pm 0.02 \text{ (stat)} \pm 0.02 \text{ (syst)} \pm 0.01 (f_{\Lambda_b^0}/f_d), \\
&< 0.07 \text{ (0.08)} \text{ at } 90\% \text{ (95\%)} \text{ CL}, \\
f_{\Xi_b^0}/f_d \times \frac{\mathcal{B}(\Xi_b^0 \rightarrow K_s^0 p \pi^-)}{\mathcal{B}(B \rightarrow K_s^0 \pi^+ \pi^-)} &= 0.011 \pm 0.015 \text{ (stat)} \pm 0.005 \text{ (syst)}, \\
&< 0.03 \text{ (0.04)} \text{ at } 90\% \text{ (95\%)} \text{ CL}, \\
f_{\Xi_b^0}/f_d \times \frac{\mathcal{B}(\Xi_b^0 \rightarrow K_s^0 p K^-)}{\mathcal{B}(B \rightarrow K_s^0 \pi^+ \pi^-)} &= 0.012 \pm 0.007 \text{ (stat)} \pm 0.004 \text{ (syst)}, \\
&< 0.02 \text{ (0.03)} \text{ at } 90\% \text{ (95\%)} \text{ CL}, \\
\frac{\mathcal{B}(\Lambda_b^0 \rightarrow \Lambda_c^+(\rightarrow p K_s^0) \pi^-)}{\mathcal{B}(B \rightarrow K_s^0 \pi^+ \pi^-)} &= 2.83 \pm 0.13 \text{ (stat)} \pm 0.16 \text{ (syst)} \pm 0.77 (f_{\Lambda_b^0}/f_d), \\
\frac{\mathcal{B}(\Lambda_b^0 \rightarrow \Lambda_c^+(\rightarrow p K_s^0) K^-)}{\mathcal{B}(B \rightarrow K_s^0 \pi^+ \pi^-)} &= 0.17 \pm 0.02 \text{ (stat)} \pm 0.01 \text{ (syst)} \pm 0.05 (f_{\Lambda_b^0}/f_d), \\
\frac{\mathcal{B}(\Lambda_b^0 \rightarrow D_s^-(\rightarrow K_s^0 K^-) p)}{\mathcal{B}(B \rightarrow K_s^0 \pi^+ \pi^-)} &= 0.040 \pm 0.021 \text{ (stat)} \pm 0.003 \text{ (syst)} \pm 0.011 (f_{\Lambda_b^0}/f_d), \\
&< 0.07 \text{ (0.08)} \text{ at } 90\% \text{ (95\%)} \text{ CL}.
\end{aligned}$$

The relative branching fraction of $\Lambda_b^0 \rightarrow \Lambda_c^+ K^-$ and $\Lambda_b^0 \rightarrow \Lambda_c^+ \pi^-$ decays is

$$\frac{\mathcal{B}(\Lambda_b^0 \rightarrow \Lambda_c^+ K^-)}{\mathcal{B}(\Lambda_b^0 \rightarrow \Lambda_c^+ \pi^-)} = 0.059 \pm 0.007 \text{ (stat)} \pm 0.004 \text{ (syst)}.$$

This result is in agreement with a recent, more precise measurement [7], from which it is independent, up to a negligible correlation in the systematic uncertainty due to particle identification efficiencies. The absolute branching fractions are calculated using the measured branching fraction of the normalisation channel $\mathcal{B}(B^0 \rightarrow K^0 \pi^+ \pi^-) = (4.96 \pm 0.20) \times 10^{-5}$ [1]. The results are expressed in terms of final states containing either

K^0 or \bar{K}^0 mesons, according to the expectation for each decay,

$$\begin{aligned}
\mathcal{B}(\Lambda_b^0 \rightarrow \bar{K}^0 p \pi^-) &= (1.26 \pm 0.19 \pm 0.09 \pm 0.34 \pm 0.05) \times 10^{-5}, \\
\mathcal{B}(\Lambda_b^0 \rightarrow K^0 p K^-) &= (1.8 \pm 1.2 \pm 0.8 \pm 0.5 \pm 0.1) \times 10^{-6}, \\
&< 3.5 \text{ (4.0)} \times 10^{-6} \text{ at 90\% (95\%) CL}, \\
f_{\Xi_b^0}/f_d \times \mathcal{B}(\Xi_b^0 \rightarrow \bar{K}^0 p \pi^-) &= (0.6 \pm 0.7 \pm 0.2) \times 10^{-6} \\
&< 1.6 \text{ (1.8)} \times 10^{-6} \text{ at 90\% (95\%) CL}, \\
f_{\Xi_b^0}/f_d \times \mathcal{B}(\Xi_b^0 \rightarrow \bar{K}^0 p K^-) &= (0.6 \pm 0.4 \pm 0.2) \times 10^{-6}, \\
&< 1.1 \text{ (1.2)} \times 10^{-6} \text{ at 90\% (95\%) CL}, \\
\mathcal{B}(\Lambda_b^0 \rightarrow \Lambda_c^+ (\rightarrow p \bar{K}^0) \pi^-) &= (1.40 \pm 0.07 \pm 0.08 \pm 0.38 \pm 0.06) \times 10^{-4}, \\
\mathcal{B}(\Lambda_b^0 \rightarrow \Lambda_c^+ (\rightarrow p \bar{K}^0) K^-) &= (0.83 \pm 0.10 \pm 0.06 \pm 0.23 \pm 0.03) \times 10^{-5}, \\
\mathcal{B}(\Lambda_b^0 \rightarrow D_s^- (\rightarrow K^0 K^-) p) &= (2.0 \pm 1.1 \pm 0.2 \pm 0.5 \pm 0.1) \times 10^{-6}, \\
&< 3.5 \text{ (3.9)} \times 10^{-6} \text{ at 90\% (95\%) CL},
\end{aligned}$$

where, for the Λ_b^0 decays, the first uncertainty is statistical, the second systematic, the third from $f_{\Lambda_b^0}/f_d$ and the last due to the uncertainty on $\mathcal{B}(B^0 \rightarrow K^0 \pi^+ \pi^-)$. For the Ξ_b^0 decays the unknown ratio of fragmentation fractions $f_{\Xi_b^0}/f_d$ is factored out, and the normalisation channel uncertainty is negligible and is therefore not included.

The $\Lambda_b^0 \rightarrow \Lambda_c^+ h^-$ absolute branching fractions can be determined more precisely than the product branching fractions with $\Lambda_c^+ \rightarrow p \bar{K}^0$, since $\mathcal{B}(\Lambda_c^+ \rightarrow p \bar{K}^0)/\mathcal{B}(\Lambda_c^+ \rightarrow p K^- \pi^+)$ is known to better precision [1] than the absolute value of $\mathcal{B}(\Lambda_c^+ \rightarrow p K^- \pi^+)$ that dominates the uncertainty on $f_{\Lambda_b^0}/f_d$. Dividing the product branching fractions quoted above by $\mathcal{B}(\Lambda_c^+ \rightarrow p K^- \pi^+)$ and by the ratio of Λ_c^+ branching fractions gives

$$\begin{aligned}
\mathcal{B}(\Lambda_b^0 \rightarrow \Lambda_c^+ \pi^-) &= (5.97 \pm 0.28 \pm 0.34 \pm 0.70 \pm 0.24) \times 10^{-3}, \\
\mathcal{B}(\Lambda_b^0 \rightarrow \Lambda_c^+ K^-) &= (3.55 \pm 0.44 \pm 0.24 \pm 0.41 \pm 0.14) \times 10^{-4}.
\end{aligned}$$

Similarly, the known value of $\mathcal{B}(D_s^- \rightarrow K_s^0 K^-)$ [1] can be used to obtain

$$\begin{aligned}
\mathcal{B}(\Lambda_b^0 \rightarrow D_s^- p) &= (2.7 \pm 1.4 \pm 0.2 \pm 0.7 \pm 0.1 \pm 0.1) \times 10^{-4}, \\
&< 4.8 \text{ (5.3)} \times 10^{-4} \text{ at 90\% (95\%) CL},
\end{aligned}$$

where the last uncertainty is due to the uncertainty on $\mathcal{B}(D_s^- \rightarrow K_s^0 K^-)$.

7 Direct CP asymmetry

The significant signal observed for the $\Lambda_b^0 \rightarrow K_s^0 p \pi^-$ channel allows a measurement of its CP asymmetry integrated over phase-space. The simultaneous extended maximum likelihood fit is modified to allow the determination of the raw asymmetry, defined as

$$\mathcal{A}_{CP}^{\text{RAW}} = \frac{N_{\bar{f}} - N_f}{N_{\bar{f}} + N_f}, \quad (6)$$

where $N_{\bar{f}/f}$ is the observed yield for $\Lambda_b^0/\bar{\Lambda}_b^0$ decays. To obtain the physical CP asymmetry, this has to be corrected for small detection (\mathcal{A}_D) and production (\mathcal{A}_P) asymmetries, $\mathcal{A}_{CP} = \mathcal{A}_{CP}^{\text{RAW}} - \mathcal{A}_P - \mathcal{A}_D$. This can be conveniently achieved with $\Lambda_b^0 \rightarrow \Lambda_c^+(\rightarrow pK_s^0)\pi^-$ decays, which share the same final state as the mode of interest, and have negligible expected CP violation.

The measured inclusive raw asymmetry for $\Lambda_b^0 \rightarrow \Lambda_c^+(\rightarrow pK_s^0)\pi^-$ decays is found to be $\mathcal{A}_{CP}^{\text{RAW}} = -0.047 \pm 0.027$, indicating that the combined detection and production asymmetry is at the few percent level. The fitted raw asymmetry for $\Lambda_b^0 \rightarrow K_s^0 p \pi^-$ decays is $\mathcal{A}_{CP}^{\text{RAW}} = 0.17 \pm 0.13$, where the uncertainty is statistical only. The raw asymmetry for each of the background components is found to be consistent with zero, as expected.

Several sources of systematic uncertainties are considered. The uncertainty on $\mathcal{A}_P + \mathcal{A}_D$ comes directly from the result of the fit to $\Lambda_b^0 \rightarrow \Lambda_c^+(\rightarrow pK_s^0)\pi^-$ decays. The effect of variations of the detection asymmetry with the decay kinematics, which can be slightly different for reconstructed $\Lambda_b^0 \rightarrow K_s^0 p \pi^-$ and $\Lambda_b^0 \rightarrow \Lambda_c^+(\rightarrow pK_s^0)\pi^-$ decays, is negligible. The possible variation of the CP asymmetry across the phase-space of the $\Lambda_b^0 \rightarrow K_s^0 p \pi^-$ decay, and the non-uniform efficiency results in a systematic uncertainty that is evaluated by weighting events using the *sPlot* technique and obtaining an efficiency-corrected value of $\mathcal{A}_{CP}^{\text{RAW}}$. The 0.003 difference with respect to the nominal value is assigned as uncertainty. Effects related to the choices of signal and background models, and possible intrinsic fit biases, are evaluated in a similar way as for the branching fraction measurements, leading to an uncertainty of 0.001. These uncertainties are summed in quadrature to yield the total systematic uncertainty.

The phase-space integrated CP asymmetry is found to be

$$\mathcal{A}^{CP}(\Lambda_b^0 \rightarrow K_s^0 p \pi^-) = 0.22 \pm 0.13 \text{ (stat)} \pm 0.03 \text{ (syst)},$$

which is consistent with zero.

8 Conclusions

Using a data sample collected by the LHCb experiment corresponding to an integrated luminosity of 1.0 fb^{-1} of pp collisions at $\sqrt{s} = 7 \text{ TeV}$, searches for the three-body charmless decay modes $\Lambda_b^0(\Xi_b^0) \rightarrow K_s^0 p \pi^-$ and $\Lambda_b^0(\Xi_b^0) \rightarrow K_s^0 p K^-$ are performed. Decays with intermediate charmed hadrons giving the same final state are also investigated. The decay channel $\Lambda_b^0 \rightarrow K_s^0 p \pi^-$ is observed for the first time, with a significance of 8.6σ , allowing a measurement of its phase-space integrated CP asymmetry, which shows no significant deviation from zero. All presented results, except for those of the branching fractions of $\Lambda_b^0 \rightarrow \Lambda_c^+ \pi^-$ and $\Lambda_b^0 \rightarrow \Lambda_c^+ K^-$, are the first to date. The first observation of a charmless three-body decay of a b baryon opens a new field of possible amplitude analyses and CP violation measurements that will be of great interest to study with larger data samples.

Acknowledgements

We express our gratitude to our colleagues in the CERN accelerator departments for the excellent performance of the LHC. We thank the technical and administrative staff at the LHCb institutes. We acknowledge support from CERN and from the national agencies: CAPES, CNPq, FAPERJ and FINEP (Brazil); NSFC (China); CNRS/IN2P3 and Region Auvergne (France); BMBF, DFG, HGF and MPG (Germany); SFI (Ireland); INFN (Italy); FOM and NWO (The Netherlands); SCSR (Poland); MEN/IFA (Romania); MinES, Rosatom, RFBR and NRC “Kurchatov Institute” (Russia); MinECo, XuntaGal and GENCAT (Spain); SNSF and SER (Switzerland); NAS Ukraine (Ukraine); STFC (United Kingdom); NSF (USA). We also acknowledge the support received from the ERC under FP7. The Tier1 computing centres are supported by IN2P3 (France), KIT and BMBF (Germany), INFN (Italy), NWO and SURF (The Netherlands), PIC (Spain), GridPP (United Kingdom). We are indebted to the communities behind the multiple open source software packages we depend on. We are also thankful for the computing resources and the access to software R&D tools provided by Yandex LLC (Russia).

References

- [1] Particle Data Group, J. Beringer *et al.*, *Review of particle physics*, Phys. Rev. **D86** (2012) 010001, and 2013 partial update for the 2014 edition.
- [2] I. Bediaga *et al.*, *On a CP anisotropy measurement in the Dalitz plot*, Phys. Rev. **D80** (2009) 096006, [arXiv:0905.4233](#).
- [3] M. Williams, *Observing CP violation in many-body decays*, Phys. Rev. **D84** (2011) 054015, [arXiv:1105.5338](#).
- [4] LHCb collaboration, R. Aaij *et al.*, *Measurement of CP violation in the phase space of $B^\pm \rightarrow K^\pm \pi^+ \pi^-$ and $B^\pm \rightarrow K^\pm K^+ K^-$* , Phys. Rev. Lett. **111** (2013) 101801, [arXiv:1306.1246](#).
- [5] LHCb collaboration, R. Aaij *et al.*, *Measurement of CP violation in the phase space of $B^\pm \rightarrow K^+ K^- \pi^\pm$ and $B^\pm \rightarrow \pi^+ \pi^- \pi^\pm$ decays*, Phys. Rev. Lett. **112** (2014) 011801, [arXiv:1310.4740](#).
- [6] LHCb collaboration, R. Aaij *et al.*, *Study of $B_{(s)}^0 \rightarrow K_s^0 h^+ h^-$ decays with first observation of $B_s^0 \rightarrow K_s^0 K^\pm \pi^\mp$ and $B_s^0 \rightarrow K_s^0 \pi^+ \pi^-$* , JHEP **10** (2013) 143, [arXiv:1307.7648](#).
- [7] LHCb collaboration, R. Aaij *et al.*, *Study of beauty baryon decays to $D^0 p h^-$ and $\Lambda_c^+ h^-$ final states*, [arXiv:1311.4823](#), to appear in Phys. Rev. D.
- [8] LHCb collaboration, R. Aaij *et al.*, *Measurements of the branching fractions of the decays $B_s^0 \rightarrow D_s^\mp K^\pm$ and $B_s^0 \rightarrow D_s^- \pi^+$* , JHEP **06** (2012) 115, [arXiv:1204.1237](#).

- [9] Belle collaboration, A. Garmash *et al.*, *Dalitz analysis of three-body charmless $B^0 \rightarrow K^0\pi^+\pi^-$ decay*, Phys. Rev. **D75** (2007) 012006, arXiv:hep-ex/0610081.
- [10] BaBar collaboration, B. Aubert *et al.*, *Time-dependent amplitude analysis of $B^0 \rightarrow K_S^0\pi^+\pi^-$* , Phys. Rev. **D80** (2009) 112001, arXiv:0905.3615.
- [11] LHCb collaboration, R. Aaij *et al.*, *Measurement of b hadron production fractions in 7 TeV pp collisions*, Phys. Rev. **D85** (2012) 032008, arXiv:1111.2357.
- [12] LHCb collaboration, R. Aaij *et al.*, *Measurement of the fragmentation fraction ratio f_s/f_d and its dependence on B meson kinematics*, JHEP **04** (2013) 1, arXiv:1301.5286.
- [13] LHCb collaboration, *Updated average f_s/f_d b -hadron production fraction ratio for 7 TeV pp collisions*, LHCb-CONF-2013-011.
- [14] Heavy Flavor Averaging Group, Y. Amhis *et al.*, *Averages of b -hadron, c -hadron, and τ -lepton properties as of early 2012*, arXiv:1207.1158, updated results and plots available at <http://www.slac.stanford.edu/xorg/hfag/>.
- [15] LHCb collaboration, A. A. Alves Jr. *et al.*, *The LHCb detector at the LHC*, JINST **3** (2008) S08005.
- [16] M. Adinolfi *et al.*, *Performance of the LHCb RICH detector at the LHC*, Eur. Phys. J. **C73** (2013) 2431, arXiv:1211.6759.
- [17] A. A. Alves Jr. *et al.*, *Performance of the LHCb muon system*, JINST **8** (2013) P02022, arXiv:1211.1346.
- [18] R. Aaij *et al.*, *The LHCb trigger and its performance in 2011*, JINST **8** (2013) P04022, arXiv:1211.3055.
- [19] T. Sjöstrand, S. Mrenna, and P. Skands, *PYTHIA 6.4 physics and manual*, JHEP **05** (2006) 026, arXiv:hep-ph/0603175.
- [20] I. Belyaev *et al.*, *Handling of the generation of primary events in GAUSS, the LHCb simulation framework*, Nuclear Science Symposium Conference Record (NSS/MIC) **IEEE** (2010) 1155.
- [21] D. J. Lange, *The EvtGen particle decay simulation package*, Nucl. Instrum. Meth. **A462** (2001) 152.
- [22] P. Golonka and Z. Was, *PHOTOS Monte Carlo: a precision tool for QED corrections in Z and W decays*, Eur. Phys. J. **C45** (2006) 97, arXiv:hep-ph/0506026.
- [23] Geant4 collaboration, J. Allison *et al.*, *Geant4 developments and applications*, IEEE Trans. Nucl. Sci. **53** (2006) 270; Geant4 collaboration, S. Agostinelli *et al.*, *Geant4: a simulation toolkit*, Nucl. Instrum. Meth. **A506** (2003) 250.

- [24] M. Clemencic *et al.*, *The LHCb simulation application, GAUSS: design, evolution and experience*, J. Phys. Conf. Ser. **331** (2011) 032023.
- [25] V. V. Gligorov and M. Williams, *Efficient, reliable and fast high-level triggering using a bonsai boosted decision tree*, JINST **8** (2013) P02013, [arXiv:1210.6861](#).
- [26] L. Breiman, J. H. Friedman, R. A. Olshen, and C. J. Stone, *Classification and regression trees*, Wadsworth international group, Belmont, California, USA, 1984.
- [27] R. E. Schapire and Y. Freund, *A decision-theoretic generalization of on-line learning and an application to boosting*, Jour. Comp. and Syst. Sc. **55** (1997) 119.
- [28] G. Punzi, *Sensitivity of searches for new signals and its optimization*, in *Statistical Problems in Particle Physics, Astrophysics, and Cosmology* (L. Lyons, R. Mount, and R. Reitmeyer, eds.), p. 79, 2003. [arXiv:physics/0308063](#).
- [29] LHCb collaboration, R. Aaij *et al.*, *Limits on the $B_{(s)}^0 \rightarrow J/\psi p\bar{p}$ and $B^+ \rightarrow J/\psi p\bar{p}\pi^+$ decays*, JHEP **09** (2013) 006, [arXiv:1306.4489](#).
- [30] R. Dalitz, *On the analysis of tau-meson data and the nature of the tau-meson*, Phil. Mag. **44** (1953) 1068.
- [31] LHCb collaboration, R. Aaij *et al.*, *Measurements of the $\Lambda_b^0 \rightarrow \Lambda J/\psi$ decay amplitudes and the Λ_b^0 baryon production polarisation in pp collisions at $\sqrt{s} = 7$ TeV*, Phys. Lett. **B724** (2013) 27, [arXiv:1302.5578](#).
- [32] BaBar collaboration, B. Aubert *et al.*, *An amplitude analysis of the decay $B^\pm \rightarrow \pi^\pm \pi^\pm \pi^\mp$* , Phys. Rev. **D72** (2005) 052002, [arXiv:hep-ex/0507025](#).
- [33] M. Pivk and F. R. Le Diberder, *sPlot: a statistical tool to unfold data distributions*, Nucl. Instrum. Meth. **A555** (2005) 356, [arXiv:physics/0402083](#).
- [34] T. Skwarnicki, *A study of the radiative cascade transitions between the Upsilon-prime and Upsilon resonances*, PhD thesis, Institute of Nuclear Physics, Krakow, 1986, DESY-F31-86-02.
- [35] ARGUS collaboration, H. Albrecht *et al.*, *Exclusive hadronic decays of B mesons*, Z. Phys. **C48** (1990) 543.
- [36] LHCb collaboration, R. Aaij *et al.*, *Precision measurement of the Λ_b^0 baryon lifetime*, Phys. Rev. Lett. **111** (2013) 102003, [arXiv:1307.2476](#).
- [37] LHCb collaboration, R. Aaij *et al.*, *Measurement of the p_T and η dependences of Λ_b^0 production and of the $\Lambda_b^0 \rightarrow \Lambda_c^+ \pi^-$ branching fraction*, LHCb-PAPER-2014-004, in preparation.